

A generalized Townsend's theory for Paschen curves in planar, cylindrical, and spherical geometries

Jeremy A. Rioussset^{a,b}, Joshua Méndez Harper^c, Josef Dufek^c, Jacob A. Engle^a, Jared P. Nelson^a, Annelisa B. Esparza^b

^a*Department of Physical Sciences, Embry-Riddle Aeronautical University, Daytona Beach, FL, 32114, USA*

^b*Aerospace, Physics & Space Sciences Department, Florida Institute of Technology, Melbourne, FL, 32901, USA*

^c*Department of Earth Science, University of Oregon, Eugene OR, 97403, USA*

Abstract

In this work, we focus on plasma discharges produced between two electrodes with a high potential difference, resulting in the ionization of the neutral particles supporting a current in the gaseous medium. At low currents and low temperatures, this process can create luminescent emissions: the so-called glow and corona discharges. The parallel plate geometry used in Townsend's (1900) theory lets us develop a theoretical formalism, with explicit solutions for the critical voltage effectively reproducing experimental Paschen curves. However, most discharge processes occur in non-parallel plate geometries, such as discharges between grains or ice particles in multiphase flows. Here, we propose a generalization of the classic parallel plate configurations to concentric spherical and coaxial cylindrical geometries in Earth, Mars, Titan, and Venus atmospheres. In a spherical case, a small radius effectively represents a sharp tip rod, while larger, centimeter-scale radii represents rounded or blunted tips. Similarly, in a cylindrical case, a small radius would correspond to a thin wire. We solve continuity equations in the gap and estimate a critical

radius and minimum breakdown voltage that allows ionization of neutral gas and formation of a glow discharge. We show that glow coronæ form more easily in Mars’s low-pressure, CO₂-rich atmosphere than in Earth’s high-pressure atmosphere. Additionally, we present breakdown criteria for Titan and Venus. We further demonstrate that critical voltage minima occur at 0.5 cm·Torr for all three investigated geometries, suggesting easier initiation around millimeter-size particles in dust and water clouds and could be readily extended to examine other multiphase flows with inertial particles.

Keywords: corona, glow, electrical discharge, Paschen, Townsend, Boltzmann, lightning, flash, Mars, Earth, Venus, Titan

Plain Language Summary

In this work, we focus on plasma discharges between two electrodes with a high voltage difference. The result is a conversion of the medium from a dielectric to a conductor. At low currents and low temperatures, this process can create luminescent emissions: the so-called glow and corona discharges. We extend the parallel plate geometry developed in Townsend’s (1900) classical theory to determine the critical discharge voltages of spheres and cylinders more likely to be encountered as particles in an atmosphere. Here, we propose a generalization of the classic parallel plate configurations to concentric spheres and coaxial cylinders in Earth, Mars, Venus, and Titan atmospheres. We computationally solve the continuity equations in the gap between objects and ultimately calculate critical electric fields for self-sustained discharges. We show that glow coronæ form more easily in Mars’s low-pressure, CO₂-rich atmosphere than in Earth’s high-pressure atmosphere. Additionally, we

present breakdown criteria for Titan and Venus. We further demonstrate that critical voltage minima occur near $0.5 \text{ cm} \cdot \text{Torr}$ for all three investigated geometries, suggesting easier initiation around millimeter-size particles in dust and water clouds.

1. Introduction

The recent and planned *in-situ* exploration of planetary bodies in the solar system motivates a better understanding of electrostatic hazards under conditions relevant to each object. Specifically, the potential for discharge involves a complex interplay between atmospheric pressure variation, gas composition, realistic geometries of charged surfaces, and the presence of suspended solids in the atmosphere. The near-surface, diffuse conditions on present-day Mars may, in particular, present hazards associated with electrostatic discharges for both robotic endeavors and potential crewed missions (Yair, 2012). Furthermore, the presence (or absence) of electrical discharges could have important implications for atmospheric chemistry and habitability (Tennakone, 2016; Hess et al., 2021). Any dielectric breakdown starts when the ambient electric field E exceeds a threshold E_{th} (e.g., Raizer, 1991, p. 128), which depends on the nature of the discharge (e.g., leader, streamer, or glow) and its polarity (see e.g., Pasko, 2006, Figure 1 for discharge in air). Putative and confirmed extraterrestrial electrical discharges have been the topic of several studies (see reviews by Leblanc et al., 2008; Rioussset et al., 2020, and references therein). While most investigations have focused on lightning as a “transient, high-current electrical discharge whose path length is measured in kilometers” (Uman, 2001, p. 8 & Table 14.1), a noteworthy

few have also investigated Transient Luminous Events, TLEs (e.g., Bering et al., 2004; Dubrovin et al., 2010; Yair, 2012) and small-scale spark or glow discharges (e.g., Méndez Harper et al., 2018; Méndez Harper et al., 2021). Elucidating discharge criteria on extraterrestrial environments is complicated by a profound dearth of *in-situ* observational data. In the context of Mars, for example, the unfortunate fate of ExoMars’ Schiaparelli module (Déprez et al., 2014) prevented the first direct measurements of the electric field at the surface of the planet. Insight into the atmospheric electrical environment on Venus and Titan, the two other rocky worlds in our solar systems with atmospheres thick enough to support gas breakdown, is also scant. Consequently, indirect measurements and analogies remain the only ways to gain insight into breakdown processes in planetary atmospheres.

The diverse span of atmospheric conditions on worlds in our own solar system suggests that the criteria that lead to breakdown in extraterrestrial environments may be equally disparate. Although both Mars and Venus host CO₂-rich atmospheres, Venus maintains a near-surface atmospheric pressure $\sim 10^4$ times higher than the Martian one (Zasova et al., 2007; Jakosky et al., 2015a,b; Sánchez-Lavega et al., 2017). On Titan, the atmospheric surface pressure is only slightly higher than Earth’s. However, Titan’s atmosphere is 4 times denser than Earth’s and significantly colder (90 K for Titan v. 287 K for Earth (Hörst, 2017)). Important chemical differences between worlds exist, too. Methane, for instance, is an important constituent of Titan’s nitrogen-rich atmosphere. Oxygen, while abundant in Earth’s atmosphere, exists in trace amounts or is absent in the atmospheres of the other three worlds. Likewise there is significant variability in the composition, abundance,

and presence of particulates in these atmospheres (e.g. silicate dust, ice, hydrocarbons), and multiphase topologies may also be important for local discharge events. Using this diversity of atmospheric conditions (summarized in Table 1), we revisit Townsend’s (1900) seminal model for self-sustained dielectrical breakdown between parallel electrodes. Townsend developed the theory supporting what is now known as Paschen’s (1889) law. Paschen’s law states that the breakdown voltage between two electrodes is a function of the product of the pressure, p , and interelectrode distance, d . Townsend (1900) proved that this scaling law comes from the exponential increase of electron number density via avalanche multiplication and secondary ionization (e.g., Bazelyan and Raizer, 1998, pp. 31–32). Interestingly, these early studies already involved experiments in air, carbon dioxide, and hydrogen. These gases contribute significantly to many planetary atmospheres in our solar system, demonstrating that discharge processes are highly dependent on gas composition.

The elegance of Townsend’s theory rests in its simplicity and the sole requirement of an exponential approximation for the effective ionization coefficient α . We revisit Townsend’s theory from first principles in Section 2. Townsend’s theory, however, assumes that the discharge occurs between two infinite parallel plates (i.e., a 1-D Cartesian geometry). To approach this configuration, experimental setups have adopted large flat electrodes with large radii R , and small gap size, d , so that $R \gg d$ (e.g., Raizer, 1991, p. 53; Lowke and D’Alessandro, 2003; Stumbo, 2013). While such configurations are suitable for laboratory experiments, they may not be representative of real discharge processes that invariably deal with complex

geometries. In fact, natural electrical discharge events are almost always associated with multiphase flows. For instance, discharges on Mars may occur between small sand grains. Similarly, arcing could occur between two voltage-carrying conductors under appropriate pressure-distance products. Thus, in the remainder of Section 2, we demonstrate that an extension to cylindrical and spherical geometries is possible for Townsend’s theory provided one approximates the mobility μ . We further develop a generalized Townsend’s criterion for the ignition of self-sustained gas discharges for coaxial cylinders and concentric spheres. We show that the numerical solutions of these equations yield the critical potential V_{cr} and corresponding electric field

	Earth	Mars	Titan	Venus	
Molar fraction	Ar	9.05×10^{-3}	1.60×10^{-2}	2.4×10^{-2}	–
	CH ₄	–	–	2.7×10^{-2}	–
	CO	1.84×10^{-7}	–	–	–
	CO ₂	3.79×10^{-3}	95.7×10^{-2}	–	96.2×10^{-2}
	He	5.04×10^{-6}	–	–	–
	N ₂	75.68×10^{-2}	2.7×10^{-2}	94.9×10^{-2}	3.5×10^{-2}
	N ₂ O	3.43×10^{-7}	–	–	–
	O ₂	20.30×10^{-2}	–	–	–
	O ₃	3.01×10^{-8}	–	–	–
	T (K)	273.04	231.2	93.9	737
N (m ⁻³)	2.688×10^{25}	1.889×10^{23}	1.150×10^{26}	9.131×10^{26}	
Coeff.	A (10^{-20}m^2)	1.04	2.11	2.14	1.42
	B (Td ⁻¹)	596.8	594.3	602.5	723.4
	C ($10^{24}/(\text{Vms})$)	3.35	12.32	12.38	3.75
	D	-0.23	-0.46	-0.46	-0.23

Table 1: Input parameters for BOLSIG runs. Atmospheric parameters are from NASA’s Global Reference Atmospheric Models (GRAMs; EarthGRAM by Leslie (2008), MarsGRAM by Justh et al. (2010), TitanGRAM by Justh and Hoffman (2020), and VenusGRAM by Justh and Dwyer Cianciolo (2021)) taken at the surface $z=0$ km on January 1st, 2000, 1200 UT, at 0° latitude and 0° longitude. These are the same surface conditions as in (RiOUSset et al., 2020). The coefficients A , B , C , and D define \tilde{a}/N and $\tilde{\mu} \times N$ in (7).

E_{cr} and satisfy the same similarity laws as first introduced by Paschen (1889). Sections 3 and 4 will respectively discuss the results and implications of the new formalism, while section 5 will summarize the principal contributions of this paper.

2. Model Formulation

This section describes the model used to develop a criterion for the initiation of self-sustained glow discharge between two one-dimensional electrodes located at $r=a$ and b , where r is a coordinate along the direction normal to the surface of the electrode (Figure 1).

In the absence of free electric charges, Gauss's law for electric field \vec{E} reduces to $\nabla \cdot \vec{E} = 0$. It further simplifies into:

$$\frac{1}{r^\delta} \frac{dr^\delta E(r)}{dr} = 0, \quad (1)$$

where $\delta = 0, 1,$ and 2 for the Cartesian, cylindrical, spherical 1-D geometries displayed in Figures 1a, 1b, and 1c, respectively. If *space charges do not contribute significantly to the total electric field between the electrodes*, then:

$$E(r) = E_a \left(\frac{a}{r} \right)^\delta, \quad (2)$$

with $E_a = E(a)$ and $a \leq r \leq b$.

The ignition of an electron avalanche between two electrodes depends on the effective ionization frequency ν_i and the poorly understood secondary ionization coefficient γ (Raizer, 1991, p. 74). Townsend's effective ionization coefficient α provides a convenient description of the primary ionization per

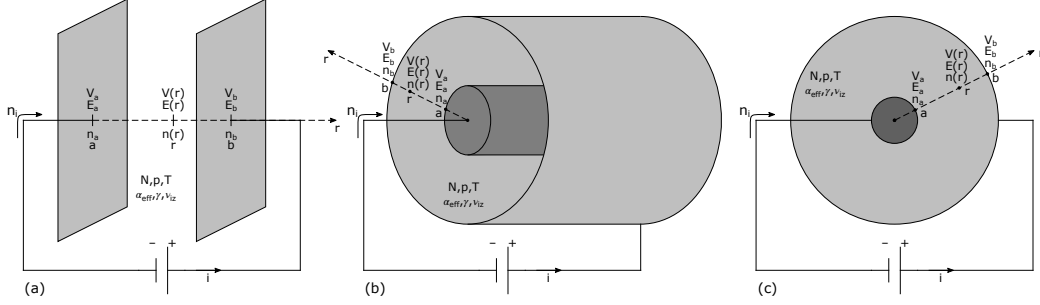


Figure 1: Townsend's discharge in one-dimensional geometries: (a) Parallel plates (Cartesian); (b) Coaxial cylindrical electrodes; (c) Concentric spherical electrodes. The gas in between the electrodes has the number density N (m^{-3}) at the temperature T (K) under the pressure p (Pa). The avalanche is characterized by Townsend's effective ionization coefficient α (m^{-1}), the secondary ionization coefficient γ , and effective ionization frequency ν_i (s^{-1}). The quantities n_i , n_a , $n(r)$, and n_b correspond to the electron density in m^{-3} carried by the electronic current i , emitted from the cathode at a , measured at r , and received at the anode at b , respectively ($a \leq r \leq b$). The corresponding electric potential and field are denoted V (V) and E (V/m).

unit length:

$$\alpha = \frac{\nu_i}{\|\vec{u}\|} = \frac{\nu_i}{u} \quad (3)$$

where the drift velocity \vec{u} depends on the mobility μ as follows (e.g., Chen, 1984, p. 66):

$$\vec{u} = \mu(E)\vec{E}. \quad (4)$$

Thus, α depends on E as follows:

$$\alpha(E) = \frac{\nu_i(E)}{\mu(E)E} \quad (5)$$

Townsend's theory provides an analytical solution to Paschen curves if α

approximately fits an exponential function:

$$\tilde{\alpha} = Ap \exp(-Bp/E), \quad (6)$$

where p is the neutral gas pressure (e.g., Raizer, 1991, pp. 149). Experimental studies typically adopt pressure-based scaling with p in Torr and α in cm^{-1} (e.g., Raizer, 1991, pp. 133) giving α/p in $1/(\text{cm} \cdot \text{Torr})$. On the other hand, theoretical investigations usually prefer density-based scaling with N , the neutral gas number density in m^{-3} and α in m^{-1} , returning α/N in m^2 (e.g., Hagelaar, 2015; Lieberman and Lichtenberg, 2005, p. 545). Both formulations are equivalent, provided that the system remains approximately at the temperature T and that the gas obeys the ideal gas law, namely $p = Nk_{\text{B}}T$, where k_{B} is the Boltzmann constant. Consequently, we can write:

$$\frac{\tilde{\alpha}}{N} = A \exp\left(-\frac{B}{E/N}\right) \quad (7a)$$

$$\tilde{\mu} \times N = C \left(\frac{E}{N}\right)^D \quad (7b)$$

where A , B , C , and D are the coefficients from a fit to the reduced Townsend's effective ionization α/N and mobility $\mu \times N$ (Figure 2) for the atmospheres considered here (Table 1).

The condition for self-sustainability of Townsend's discharges in any of the geometries shown in Figure 1 starts with the continuity equation:

$$\frac{\partial n}{\partial t} + \nabla \cdot n\vec{u} = n\nu_1 \quad (8)$$

where n is the plasma density.

Combining Equations (1), (3), and (8) in a steady state ($\partial/\partial t = 0$) yields $\frac{1}{r^\delta} \frac{d}{dr} (r^\delta n u) = n \alpha u$. Using Equation (4), this simplifies further into:

$$\frac{d \ln(r^\delta n \mu(E) E)}{dr} = \alpha(E). \quad (9)$$

From Equation (2), we have $E_a a^\delta = E_b b^\delta$. If $A_{av} = n_b/n_a$ is the avalanche coefficient defined as the ratio of the number densities $n_a = n(a)$ and $n_b = n(b)$,

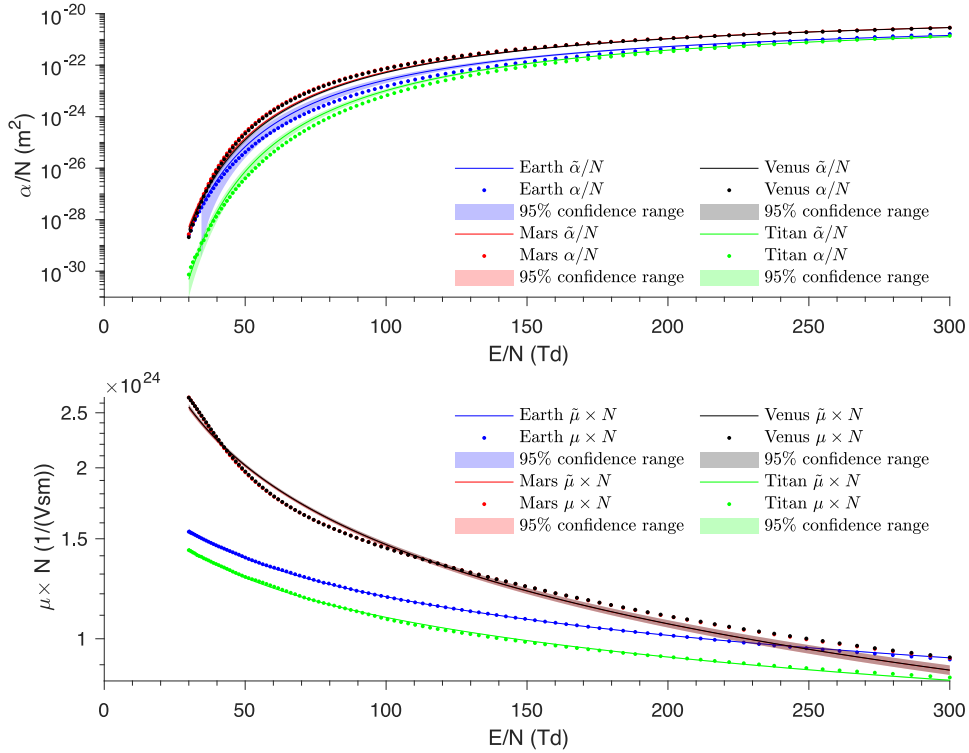


Figure 2: Scaling laws for (a) the reduced effective Townsend's ionization coefficient α/N and (b) reduced mobility $\mu \times N$ plotted against the reduced electric field E/N . Blue, red, gray, and green colors correspond to Earth-, Mars-, Venus-, and Titan-like atmospheres, respectively (see Table 1).

then Equation (9) yields:

$$A_{\text{av}} = \frac{n_b}{n_a} = \frac{\mu(E_a)}{\mu(E_b)} \exp\left(\int_a^b \alpha(E) dr\right) \quad (10)$$

2.1. Sustainability

Call n_i the number density of charges from the electronic current i and n_γ the one from secondary avalanches between the electrodes, then the conservation of charge produces the system below:

$$\begin{cases} n_a &= n_i + n_\gamma \\ n_\gamma &= \gamma(n_b - n_a) \cdot \\ n_b &= A_{\text{av}}n_a \end{cases} \quad (11)$$

An electron avalanche occurs when the ratio n_b/n_i diverges (e.g., Naidu and Kamarju, 2013, Sec. 2.5). Then, the condition for initiating a self-sustained discharge follows from Equation (8):

$$\frac{n_b}{n_i} = \frac{\frac{A_{\text{av}}}{\gamma}}{1 + \frac{1}{\gamma} - A_{\text{av}}} \rightarrow \infty, \quad (12)$$

which is satisfied when:

$$A_{\text{av}} = 1 + \frac{1}{\gamma}. \quad (13)$$

Using Equation (13) to substitute A_{av} in Equation (10) yields after simplifications:¹

$$\boxed{\int_a^b \alpha(E) dr + \ln \left(\frac{\mu(E_a)}{\mu(E_b)} \right) = \ln \left(1 + \frac{1}{\gamma} \right)}. \quad (14)$$

In all three 1-D cases, Equations (2), (7a), and (7b) let us approximate α/N and $\mu \times N$ as a function of a , r , and E_a . Thus, the condition of self-sustainability Equation (14) in the absence of space charges and displacement field becomes:

$$\int_a^b AN \exp \left(-\frac{B}{E_a/N} \left(\frac{r}{a} \right)^\delta \right) dr + D \ln \left(\left(\frac{b}{a} \right)^\delta \right) = \ln \left(1 + \frac{1}{\gamma} \right) \quad (15)$$

If A and B are converted to $1/(\text{cm} \cdot \text{Torr})$ and $V/(\text{cm} \cdot \text{Torr})$ and d is the distance between the electrodes ($b = a + d$), then we can show that the scalability of E_a/p naturally derives from Equation (15) as follows:

$$\int_0^d Ap \exp \left(-\frac{B}{E_a/p} \left(1 + \frac{pr}{pa} \right)^\delta \right) dr + D \ln \left(\left(1 + \frac{pd}{pa} \right)^\delta \right) = \ln \left(1 + \frac{1}{\gamma} \right) \quad (16)$$

The critical electric field E_{cr} is measured at $r = a$, therefore $E_{cr} = |E_a|$. Consequently, Equation (16) yields the following results for the specific

¹Note that if $E_a = E_b$ (e.g., in a parallel plate geometry), one straightforwardly retrieves the classic formula (e.g., Raizer, 1991, p. 177).

geometries described in Figure 1:

$$\exp\left(-\frac{Bp}{E_{\text{cr}}}\right) = \frac{1}{Apd} \ln\left(1 + \frac{1}{\gamma}\right) \quad \delta = 0 \quad (17a)$$

$$-\frac{E_{\text{cr}}}{Bp} \left[\exp\left(-\frac{Bp}{E_{\text{cr}}}\left(1 + \frac{pd}{pa}\right)\right) - \exp\left(-\frac{Bp}{E_{\text{cr}}}\right) \right] = \frac{1}{Apa} \ln\left(\frac{\left(1 + \frac{1}{\gamma}\right)}{\left(1 + \frac{pd}{pa}\right)^D}\right) \quad \delta = 1 \quad (17b)$$

$$\sqrt{\frac{E_{\text{cr}}}{Bp}} \left[\operatorname{erf}\left(\sqrt{\frac{E_{\text{cr}}}{Bp}}\left(1 + \frac{pd}{pa}\right)\right) - \operatorname{erf}\left(\sqrt{\frac{E_{\text{cr}}}{Bp}}\right) \right] = \frac{2}{\sqrt{\pi}} \frac{1}{Apa} \ln\left(\frac{\left(1 + \frac{1}{\gamma}\right)}{\left(1 + \frac{pd}{pa}\right)^{2D}}\right) \quad \delta = 2 \quad (17c)$$

where $\operatorname{erf}(x) = \frac{2}{\sqrt{\pi}} \int_0^x e^{-t^2} dt$ is the Gauss error function (e.g., Lipschutz et al., 2018, p. 203).

2.2. Critical voltage

Paschen curves are plots of the product pressure times density pd versus critical electric potential V_{cr} . This potential measured between the electrodes at a and b ($V_{\text{cr}} = V_b - V_a$) corresponds to the voltage necessary to initiate a self-sustained discharge and obeys the classic definition $V(r) = -\int_a^b \vec{\mathbf{E}} \cdot d\vec{\mathbf{r}}$ (e.g., Zangwill, 2019, p. 62). Equation (2) then yields V_{cr} for the three cases of Figure 1:

$$V_{\text{cr}} = E_{\text{cr}}d \quad \delta = 0 \quad (18a)$$

$$V_{\text{cr}} = E_{\text{cr}}a \cdot \ln\left(1 + \frac{d}{a}\right) \quad \delta = 1 \quad (18b)$$

$$V_{\text{cr}} = E_{\text{cr}}d \cdot \left(1 + \frac{d}{a}\right)^{-1} \quad \delta = 2 \quad (18\text{c})$$

For $\delta = 0$ (case of parallel plates), Equations (17a) and (18a) simplify into the well-established formula (e.g., Raizer, 1991, p. 133):

$$V_{\text{cr}} = \frac{Bpd}{\ln \left(\frac{Apd}{\ln \left(1 + \frac{1}{\gamma} \right)} \right)} \quad (19)$$

If Equations (17b) and (17c) had known analytical solutions, one could straightforwardly obtain solutions in the cylindrical and spherical geometries ($\delta=1$ and 2 , respectively) from Equations (18b) and (18c). In the absence of closed-form solutions, we use MATLAB `fzero` root-finding algorithm to numerically solve Equation (17) for E_{cr} given specific values of pa and pd . This function combines the bisection, secant, and inverse quadratic interpolation methods and is based on the works by Brent (1973) and Forsythe et al. (1976). We use the values of E_{cr} to deduce the critical voltage V_{cr} from Equation (18) given pa , pd , and δ .

In the next section, we present the results from our calculation as surface plots for all three geometries of Figure 1 for the environments described in Table 1. We also compare the results to experimental data from the peer-reviewed literature.

3. Results

The near-surface atmospheric breakdown criteria for Earth, Mars, Titan, and Venus are summarized in Figures 3 through 6. In each figure, columns (I) and (II) respectively display the critical electric field E_{cr} and potential V_{cr} for the various geometries explored here as functions pd and pa . The results are displayed for values of pa from 10^{-1} to 10^{+3} cm · Torr and pd from 10^{-1} to 10^{+3} cm · Torr. The use of pressure-scaled dimensions eases the comparison with experimental data in columns (III) and (IV). Therefore, Figures 3 to 6 use pressure-scaled values (E/p , pa , pd) rather than number-density scaled parameters (e.g., E/N , α/N , $\mu \times N$ in Figure 2). The conversion is possible using the neutral temperatures given in Table 1 and the ideal gas law discussed in Section 2 (see Appendix A for details).

In Figures 3 to 6, the first, second, and third rows display the results for parallel plates, coaxial cylinders, and concentric spherical electrodes, respectively. Specifically, panels (a) and (b) show the calculated values of E_{cr} and V_{cr} for the parallel plate geometry and confirm that the critical electric field and potential do not vary as a function of pa . Therefore, the surface plots effectively collapse into the well-known curves of Townsend's theory. For coaxial cylinders, panels (e) and (f), and concentric spheres, panels (i) and (j), Figures 3 to 6 exhibit a similar dependence with pd , related to the separation between the electrodes, but also introduce a new dependence on pa , emphasizing the role of the size of the system for the initiation of self-sustained glow discharge. Conventional Paschen curves have a well-defined minimum, Stoletov's point, with a potential $V_{\text{min}} = \frac{eB}{A} \ln\left(1 + \frac{1}{\gamma}\right)$

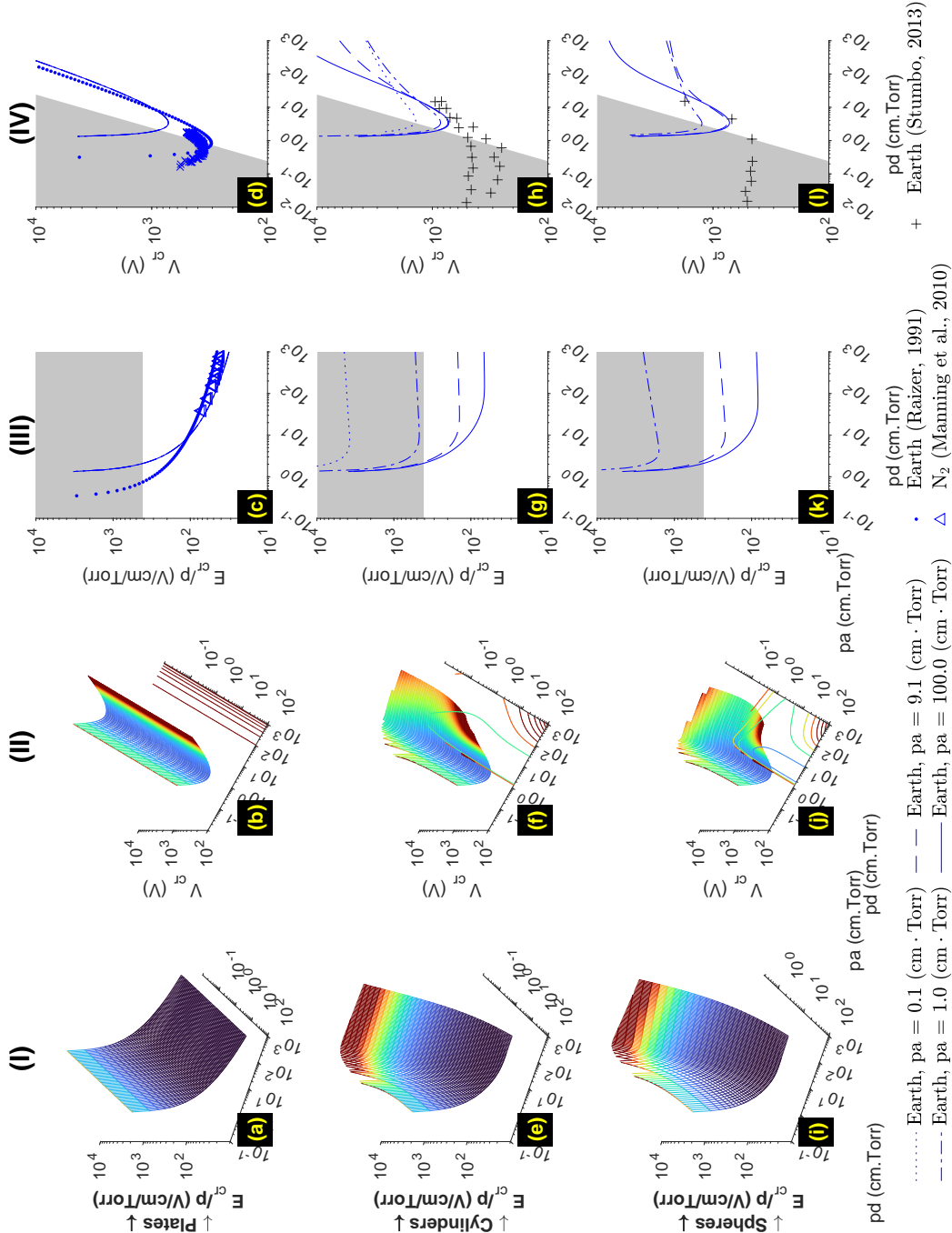


Figure 3: Breakdown criteria in the Earth-like atmosphere described in Table 1. The reduced critical electric field E_{cr}/p is displayed as a function of the reduced size of electrode pa and distance pd between electrodes a and b in column (I). Column (III) shows E_{cr}/p vs. pd for selected pa -values for comparison with experimental data. Columns (II) and (IV) are the same as columns (I) and (III) but for the critical voltage V_{cr} . The first, second, and third rows displays the results for electrodes with the following geometries: parallel plates (a-d), coaxial cylinders (e-h), and concentric spheres (i-l). The shaded areas correspond to domains where $E \geq 10E_k$.

at $pd_{\min} = \frac{e}{A} \ln\left(1 + \frac{1}{\gamma}\right)$ (e.g., Raizer, 1991, p. 134). However, this minimum point becomes a minimum curve in cylindrical and spherical geometries (panels (f) and (j) in Figures 3 to 6). As expected, the minimum of the surface plot for the parallel-plate case is independent of the value of pa and obeys Stoletov's equations for pd_{\min} and V_{\min} .

We compare our numerical results with other numerical calculations and experimental data in columns (III) and (IV) of Figures 3 to 6. There, we plot selected cross-sections from the surface plots in columns (I) and (II). Columns (III) and (IV) display E_{cr}/p and V_{cr} , respectively, as a function of the parameter pd for fixed values of pa : 0.1, 1, ~ 10 , and 100 cm·Torr. Experimental measurements in air are rendered in blue markers: \bullet and \triangle for measurements from (Raizer, 1991) and \times for Stumbo's (2013) data. Red markers display data for Mars: ∇ for Raizer's (1991) and $+$ for Manning et al.'s (2010) works. We further show data for pure CO₂ with black markers where \bullet , \square , ∇ , $+$, \times , and \triangleleft show the results from (Raizer, 1991), (Hackam, 1969), (Buhler et al., 2003), (Manning et al., 2010), (Stumbo, 2013), and (Meek and Craggs, 1953), respectively. For comparisons with Earth and Titan scenarios, we included experimental results in N₂ from (Manning et al., 2010).

As expected, self-sustained discharges between parallel plates do not depend on the parameter pa (see panels (a) and (b) across Figures 3 through 6). Interestingly, Stoletov's points visible in column (IV) occur at similar values of pd and V_{\min} ($\approx 0.1 - 1$ cm · Torr and ≈ 2 V/cm/Torr, respectively) for the various gas mixtures and geometries. Columns (III) and (IV) also show that the theoretical values from Section 2 underestimate experimental values of E_{cr} and V_{cr} for all geometries and values of pa . For a given system,

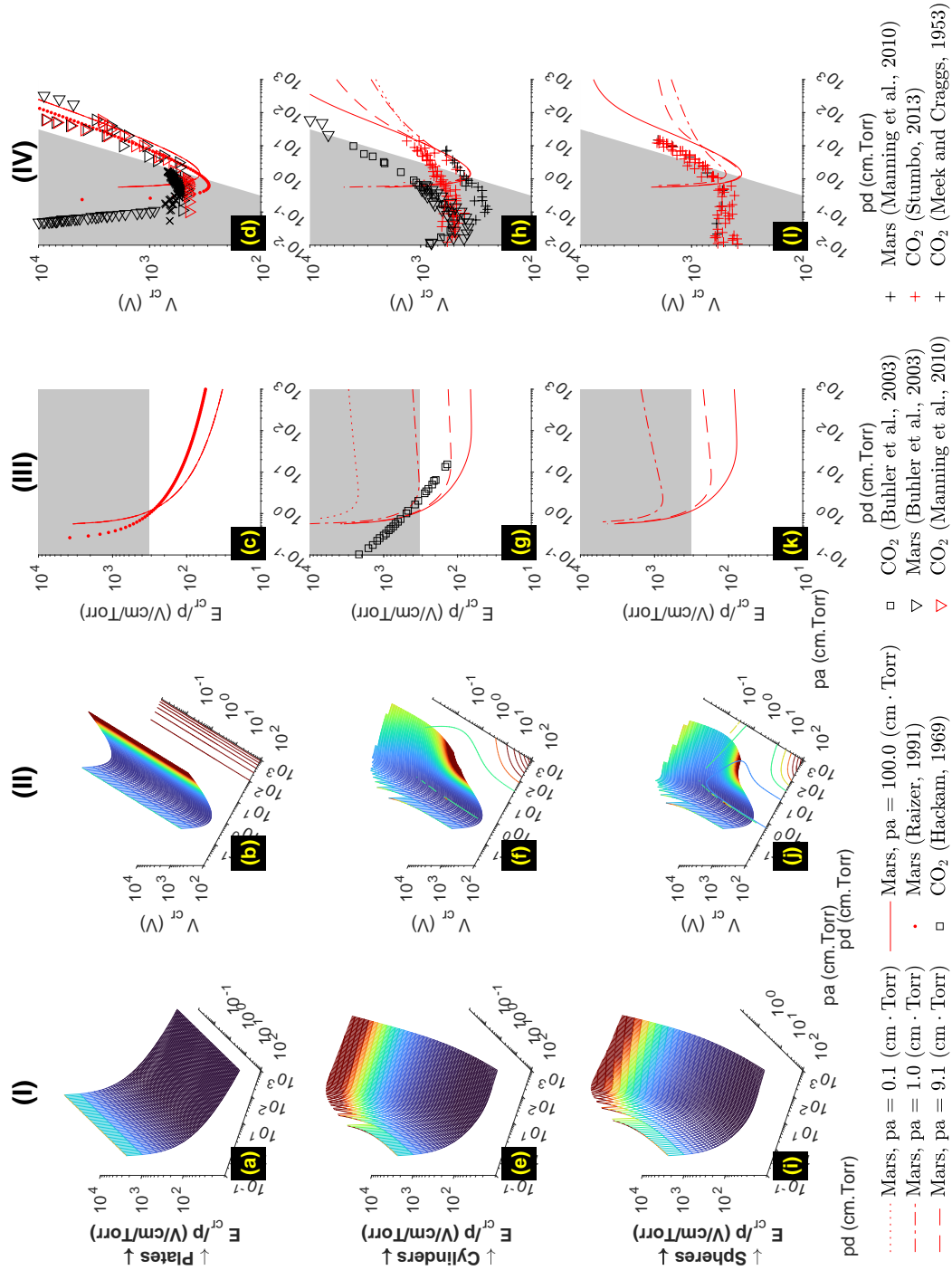


Figure 4: Same as Figure 3 for the Mars-like environment described in Table 1.

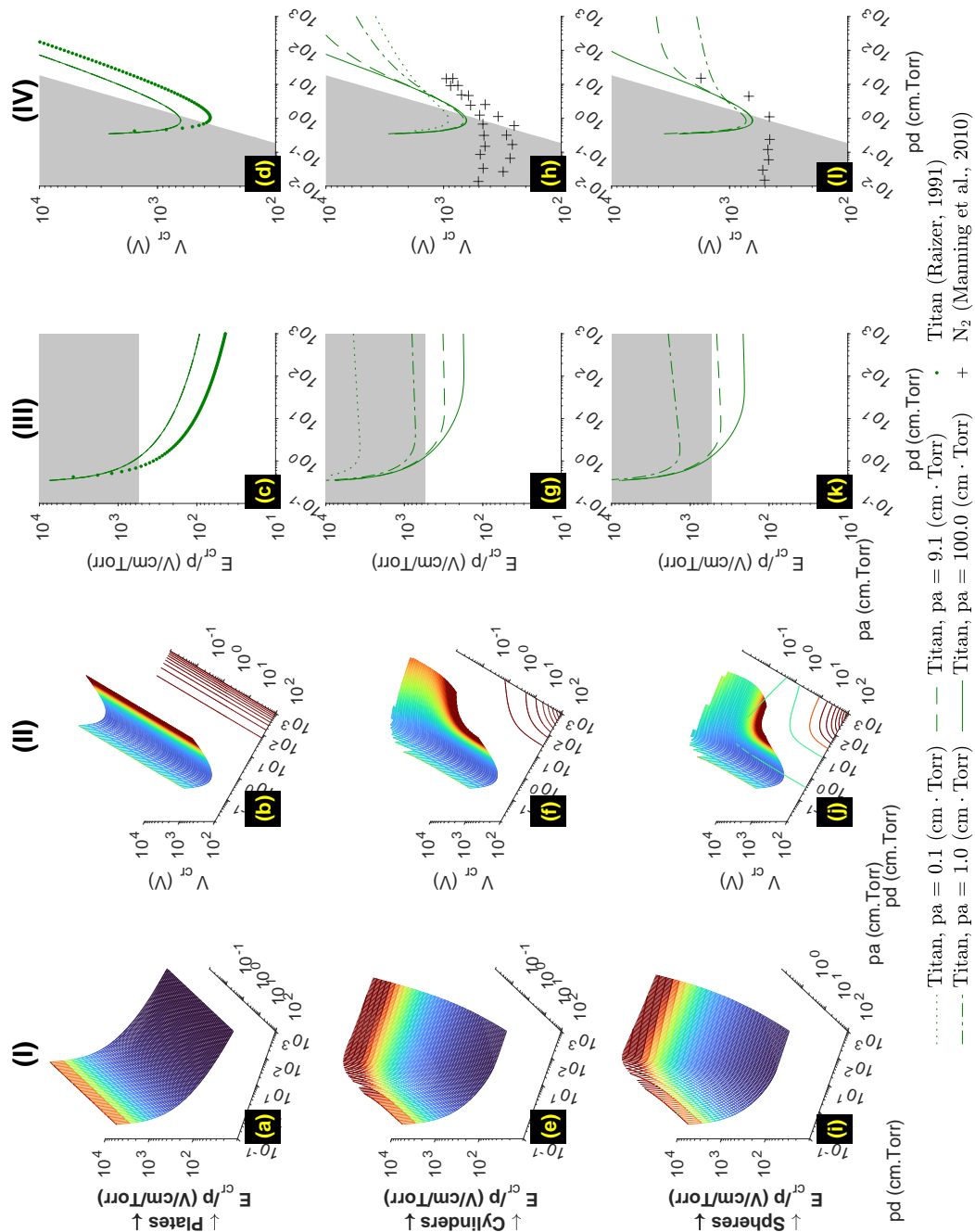


Figure 5: Same as Figure 3 for the Titan-like environment described in Table 1.

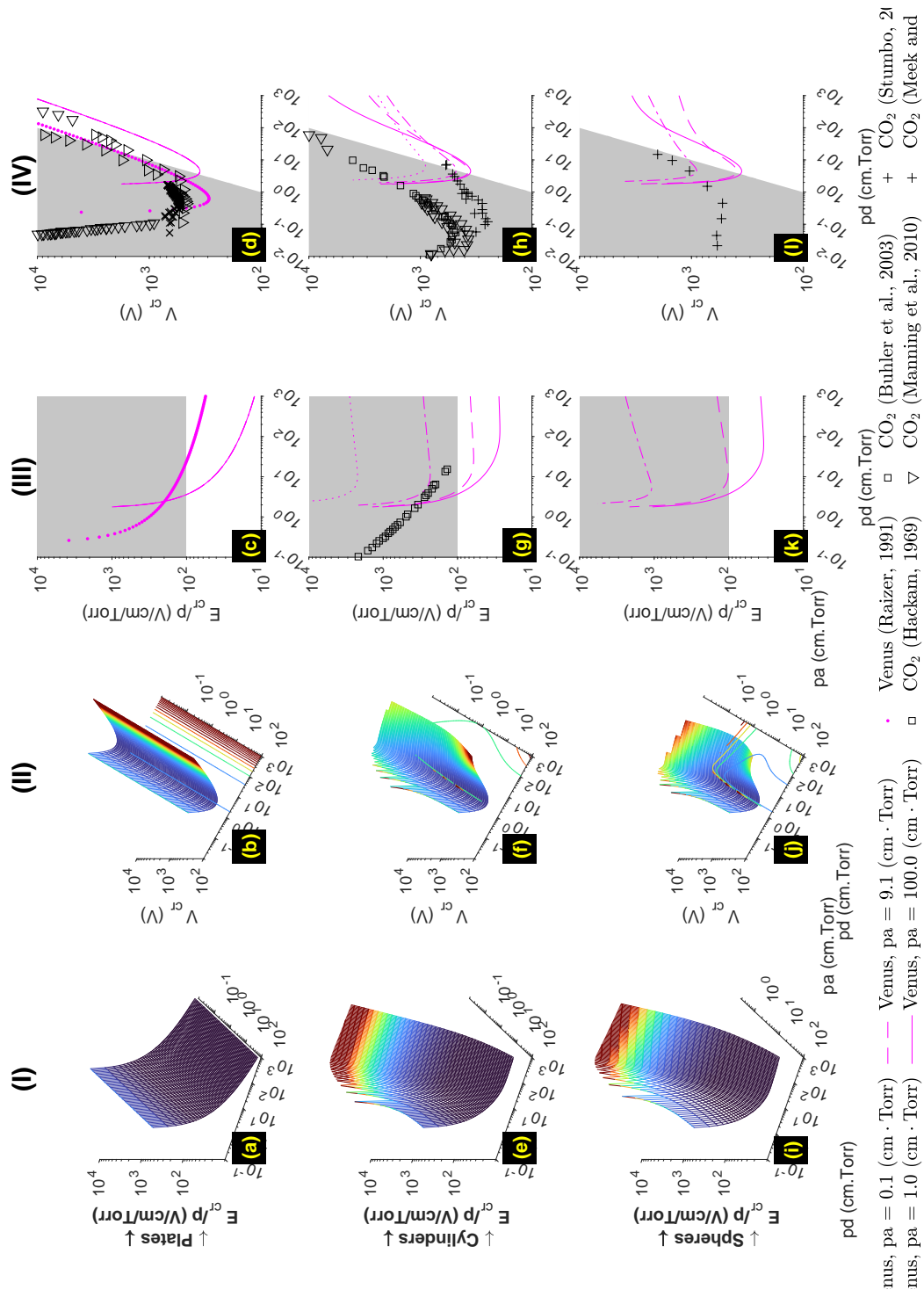


Figure 6: Same as Figure 3 for the Venus-like environment described in Table 1.

if one splits the Paschen curve around the Stoletov’s point, one can define a high electric field regime for $pd \ll pd_{\min} \approx 0.1 - 1 \text{ cm} \cdot \text{Torr}$ forming the left-hand branch of the curves and a high-pressure regime on the right-hand branch of curves for $pd \gtrsim pd_{\min}$.

The right branches of the curves show promising agreement (within an order of magnitude) between theoretical curves and measurements provided that: (1) one accounts for the uncertainty in deriving the coefficients A , B , and D ; and (2) one carefully considers the values of pa best representing the geometries of concentric or coaxial electrodes. For these reasons, we shall note that the theoretical slopes closely follow those formed by the experimental measurements from various authors (see legends of Figures 3 through 6 for details). The curves using A and B from (Raizer, 1991, p. 56 and ‘●’ markers in columns (III) and (IV)) show the influence of these coefficients on the location of Stoletov’s points in theoretical plots. While some authors have derived these values directly from the Paschen curves, we derived A , B , and D from solutions to the Boltzmann equation (see Figure 2 and Section 2) to maintain consistency of methodology across coefficients and gases. Another explanation of the aforementioned difference stems from the differences between pure gases and complex atmospheres (e.g., pure CO_2 vs. Mars atmospheres, pure N_2 vs air). Even in cases when the atmospheric composition is almost pristine (e.g., Mars’s atmosphere is $\gtrsim 95\%$ CO_2), the presence of minor components can dramatically alter the condition for discharge initiation as evidenced by Rioussset et al. (2020) in the case of conventional breakdown E_k .

4. Discussion

The results presented in Section 3 differ from previous attempts at generalizing Townsend's theory of Paschen curves mainly in their full treatment of electron mobility in the continuity equation. Neglecting the volume increase along the avalanche path, Raizer (1991, p. 177) or Meek and Craggs (1953, p. 100) straightforwardly rewrote the condition for initiation of self-sustained discharges Equation (15) as: $\int_a^b Ap \exp(-Bp/E(r)) dr = \ln(1 + 1/\gamma)$. The proposed formalism here includes the volume change as the electrons move from the inner to the outer electrode via the additional mobility term: $\ln(\mu(E_a)/\mu(E_b)) \approx D \ln((b/a)^\delta)$.

Section 2 has established the equivalence between the classic theory for parallel plate electrodes and the equations developed in this work. In addition, the revised equations are fully consistent with the well-established scaling laws. We further note that all the geometrical parameters in Equation (16) appear in a product with p (i.e., pa , pb , pr , and pd). Consequently, one must have $E_{\text{cr}} \propto p$ so that Equation (16) remains true if the pressure changes with all other parameters remaining the same. Similarly, Equation (18) establishes the invariance of the critical voltage V_{cr} through pressure changes. Writing $E_{\text{cr}} = \frac{E_{\text{cr}}}{p}p$ lets us rewrite Equations (18a), (18b), and (18c) to display the pressure scaling explicitly as follows:

$$V_{\text{cr}} = \frac{E_{\text{cr}}}{p}pa \cdot \frac{pd}{pa} \quad \delta = 0 \quad (20a)$$

$$V_{\text{cr}} = \frac{E_{\text{cr}}}{p}pa \cdot \ln \left(1 + \frac{pd}{pa} \right) \quad \delta = 1 \quad (20b)$$

$$V_{\text{cr}} = \frac{E_{\text{cr}}}{p} pa \cdot \frac{\frac{pd}{pa}}{1 + \frac{pd}{pa}} \quad \delta = 2 \quad (20c)$$

Since E_{cr}/p is constant, then V_{cr} only depends on the parameters pd (as in the classic Townsend's (1901) theory) and pa . The previously established scaling law stands with the additional parameter pa . Therefore, Equations (17) and (20) demonstrate that both the critical electric field, E_{cr} , and potential, V_{cr} , are functions of the reduced electrode and gap sizes, namely pa and pd .

Alternately, the ideal gas law, $p = Nk_{\text{B}}T$, allows us to rewrite E_{cr} and V_{cr} as functions of Nd and Na , where N is the number gas density. This result holds for constant gas temperature, which is a reasonable assumption for a cold, non-thermalized discharge such as corona or glow. However, it is worth noting that the coefficients A , B , and D are derived from a fit to the Boltzmann equation using the parameters given in Table 1. The BOLSIG+ solver (Hagelaar, 2015) requires a temperature input while it outputs reduced values for α and μ using the number density N . The pressure conversion is necessary to compare to experimental data. The temperatures we used for the four worlds are summarized in Table 1. The conversions of the coefficients from density to pressure call for the neutral gas temperature (see Appendix A) and this information is required for direct comparison between experimental and theoretical Paschen curves. Any modification to the A and B coefficients will primarily shift the curves and surfaces along the vertical V_{cr} and horizontal pd axes of Figures 3 to 6, respectively.

In all considered cases, E_{cr}/p and V_{cr} present an asymptotic behavior towards infinite electric field and potential for low values of pd , independently

of pa . The values on the left branches of the Paschen curves ($pd \lesssim pd_{\min}$ in column (IV) of Figures 3 through 6) should be taken with caution as they may not describe the physical mechanism occurring in high-electric fields. Discharges at very low pd correspond to dielectric breakdown in a quasi-vacuum. Indeed, Raizer (1991, p. 135) noticed that the electron-avalanche process responsible for self-sustained discharges between parallel plates is replaced by cathode emission at $pd \lesssim 10^{-3} \text{ cm} \cdot \text{Torr}$. Thus, the properties of the discharge are no longer defined by the neutral gas between the electrode, but rather by the metallic composition of the electrode. For this reason, the numerical solutions presented in this work do not apply in such regimes. On the other hand, the convergence across gas compositions at high pd indicates that the number density of the neutral gas can become a dominant factor over the molecular electric properties for large gaps under significant pressure. The right branches show similarities to each other across the geometries at large $pd \lesssim 100 \text{ cm} \cdot \text{Torr}$. We advance that these similarities (observed in column (IV) of Figures 3 through 6) reflect a regime where the electrode radii of curvature are large enough relative to the gap sizes to result in quasi-plane-to-plane conditions.

Considering the uncertainty of the electrode geometries in experimental data, the theoretical curves are consistent with the measurements. Both approaches indicate minima in the critical voltages around $0.5 \text{ cm} \cdot \text{Torr}$. A simple division by the atmospheric pressure returns the gap size most susceptible to trigger a self-sustained discharge in a given atmosphere. For example, under a pressure of 760 Torr (Earth's surface pressure), dielectric breakdown may occur in gaps sizes $\approx 5 \mu\text{m}$ at $V_{\text{cr}} \lesssim 500 \text{ V}$. At tropopause's

levels, $p \approx 200$ Torr and the same voltage can initiate a Townsend discharge in a larger gap ($d \approx 25 \mu\text{m}$). Similarly, the lower pressure in the Martian atmosphere indicates that larger gaps are more prone to dielectric breakdown at the surface of Mars.

Panels (f) and (j), i.e., Column (II), of Figures 3 to 6 emphasize the added role of mobility in non-planar geometries. In particular, these plots suggest that a reduced radius pa of $\approx 1 \text{ cm} \cdot \text{Torr}$ is better for initiating self-sustained glow discharges. This corresponds to radii of curvatures $a \approx 0.05/1 \text{ mm}$ for Earth and $0.2/5 \text{ mm}$ for Mars at ground and cloud levels ($z \approx 10/20 \text{ km}$) in the atmosphere. Such radii of curvature are consistent with previous theories that sharp-tipped rods should facilitate the initiation of upward-connecting leaders and result in better lightning protection, a prediction contrary to field studies (e.g., Moore, 1983; Moore et al., 2000a,b, 2003). The paradox therefore remains. However, for Earth, the previous calculations indicate that millimeter-sized ice graupels are in the ideal size range for discharge initiation at cloud altitude. Beyond meteorological multiphase flows, numerous Earth systems transport particles in these size ranges and involve discharge processes across a wide range of scales (Crozier, 1964; Kamra, 1972; Farrell et al., 2004; Cimarelli et al., 2022; Méndez Harper et al., 2022). Such flows include gravity currents (dust storms, pyroclastic density currents), volcanic eruption plumes, and wildfire smoke clouds. Particles in these contexts may have substantial inertia and granular temperatures such that transient optimal gap distances between particles should be common even in very dilute flows (Dufek et al., 2012; Dufek and Bergantz, 2007). Lastly, if corona discharge is indeed a precursor to connecting leaders, they can be

involved in the process of initiation of lightning and Transient Luminous Events (TLEs), jets and sprites in particular.

While this study provides a framework to constrain the capacity of charged surfaces to cause a breakdown on Mars, Titan, and Venus, how surfaces become electrified on these worlds remains an area of active research. Mars, for instance, lacks a hydrological cycle to drive meteorological electrical activity analogous to that on Earth. While Titan and Venus do have “hydrological” processes that involve the cycle of hydrocarbons and sulfur compounds, respectively, whether or not clouds of these compositions are propitious for discharges remains unknown (Hayes et al., 2018; Shao et al., 2020).

However, as is the case for Earth, the three other worlds considered here do host granular reservoirs that could provide pathways for non-meteorological discharges (Thomas and Gierasch, 1985; Balme and Greeley, 2006; Radebaugh et al., 2008; Lorenz and Zimbelman, 2014). Martian dust storms involve the movement of large amounts of silicate particles which invariably undergo collisions. These interactions could charge dust particles via frictional and contact electrification—collectively known as *triboelectrification* (Horányi and Lawrence, 2001; Melnik and Parrot, 1998; Merrison et al., 2004; Delory and Farrell, 2011). Indeed, a broad range of experimental efforts suggests that tribocharging may be quite efficient within Martian dust events (e.g., Eden and Vonnegut, 1973; Krauss et al., 2003; Wurm et al., 2019; Méndez Harper et al., 2021). While these experiments have investigated electrification at the grain scale, computer simulations (sometimes combined with experiments (e.g., Harrison et al., 2016)) have provided useful full-scale expedients for studies of dust devil electrification (e.g., Melnik and Parrot, 1998; Farrell

et al., 2003). The results of these studies all converge to the conclusion that electrification in Martian dust storms should suffice to produce gas breakdown and an atmospheric electric circuit (Farrell and Desch, 2001).

Similar charging processes may operate on Titan and Venus (or any other world with mobile granular materials). On Titan, triboelectrification has been associated with the transport of wind-blown hydrocarbon sand (Méndez Harper et al., 2017) and the aggregation of fine photochemical hazes. Very little work has explored triboelectrification under relevant Venusian conditions. However, the presence of dunes and volcanic features on Venus indicates particles may charge frictionally during aeolian transport and eruptions (James et al., 2008).

Determining the conditions under which atmospheric discharges occur has implications for atmospheric chemistry and habitability. Furthermore, discharges could present risks to landers and rovers or cause artifacts that confound the interpretation of sensor data (Krauss et al., 2003). Recently, for instance, calculations performed by Farrell et al. (2021) suggest that the rotors of the Ingenuity helicopter could cause localized breakdown during landing or takeoff. While videography of initial flights has not revealed visual evidence for discharges, such events may be best detected electronically. Unfortunately, Ingenuity does not have the instrumentation to make such measurements. The upcoming Dragonfly rotorcraft mission to Titan, however, will involve an electric field measurement system (EFIELD) in its DraGMet suite. The main objective of the EFIELD experiments is to measure Schumann resonances, which, if detected, would provide evidence for lightning. Beyond ELF modes, Chatain et al. (2022) have made a compelling case that the sensor could be

used to detect the movement of charged hydrocarbon sand flying past or impinging on the probe during “brownout” conditions. Because (by definition) discharges also involve the movement of charge, the EFIELD instrument could, in principle, detect small-scale breakdown in the vicinity of the rotorcraft. In the case of Venus, near-term investigations of discharges in the Venusian environment will remain limited to remote sensing observations and analog experiments.

5. Conclusions

The principal results and contributions from this work can be summarized as follows:

1. The theoretical treatment of self-sustained discharge between coaxial cylinders or concentric spheres requires a model of mobility. The reduced electron mobility in telluric world atmospheres approximately follows a power law: $\tilde{\mu} \times N = C(E/N)^D$, where C and D are gas-specific constants derived from a numerical fit to the curve E/N vs. $\mu \times N$.
2. The newly proposed formalism explains the slope of the Paschen curves in non-planar geometries and maintains the scaling laws established by the classic theory.
3. In cylindrical and spherical cases, both electrode and gap sizes define the condition of discharge initiation. Thus, Paschen curves and Stoletov’s points become surfaces and curves, respectively.
4. Critical voltages occur at pd and $pa \approx 0.5 \text{ cm} \cdot \text{Torr}$, suggesting easier initiation around millimeter-size particles in dust and water clouds.

5. Glow corona formation is easier in Mars low pressure, CO₂-rich atmosphere than in Earth's high-pressure atmosphere.

The specific values of the fit coefficients need revising based on laboratory experiments rather than numerical experiments (i.e., solution of the Boltzmann equation) and will be addressed in future work.

Appendix A. Density vs. pressure scaling

Experimental work typically adopts pressure-scaled variable, E/p , α/p , $\mu \times p$ (e.g., columns (III) and (IV) in Figures 3 to 6), while numerical solvers conventionally prefer the number density N as the scaling factor. Calculations of the fit coefficients A , B , C , and D are performed using numerical solutions but require conversion for comparison with the peer-reviewed experimental data. Equations (A.1) to (A.3) provide the conversion factors.

$$\frac{\alpha}{p} = \left(\frac{101325}{100 \cdot 760} \cdot \frac{1}{k_B T} \right) \frac{\alpha}{N} \quad (\text{A.1})$$

$$\mu \times p = \left(\frac{10^4 \times 760}{101325} \cdot k_B T \right) \mu \times N \quad (\text{A.2})$$

$$\frac{E}{p} = \left(\frac{101325 \cdot 10^{-21}}{100 \cdot 760} \cdot \frac{1}{k_B T} \right) \frac{E}{N} \quad (\text{A.3})$$

where the variables have the units indicated in parentheses: α/p (1/(cm · Torr)), $\mu \times p$ ((cm² · Torr) / (V · s)), E/p (V/(cm · Torr)), α/N (m²), $\mu \times N$ (1/(V · m · s)), E/N (Td), k_B (J/K), and T (K), respectively.

Similarly, the fit coefficients A and B need converting. If indices p and N

indicate the variables used for density and pressure calculations, then:

$$A_p = \left(\frac{101325}{100 \cdot 760} \cdot \frac{1}{k_B T} \right) A_N \quad (\text{A.4})$$

$$B_p = \left(\frac{101325 \cdot 10^{-21}}{100 \cdot 760} \cdot \frac{1}{k_B T} \right) B_N \quad (\text{A.5})$$

The coefficient D is unchanged, while C cancels out from the equations and requires no conversion.

Acknowledgment

This work was supported by the National Science Foundation (grant number: 2047863), Embry-Riddle Aeronautical University Office of Undergraduate Research.

References

- Balme, M., Greeley, R., 2006. Dust devils on Earth and Mars. *Rev. Geophys.* 44. doi:10.1029/2005rg000188.
- Bazelyan, E.M., Raizer, Y.P., 1998. *Spark Discharge*. Chemical Rubber Company Press, New York, NY.
- Bering, E.A., Benbrook, J.R., Bhusal, L., Garrett, J.A., Paredes, A.M., Wescott, E.M., Moudry, D.R., Sentman, D.D., Stenbaek-Nielsen, H.C., Lyons, W.A., 2004. Observations of transient luminous events (TLEs) associated with negative cloud to ground (-CG) lightning strokes. *Geophys. Res. Lett.* 31. doi:10.1029/2003GL018659. 105104.

- Brent, R.P., 1973. Algorithms for Minimisation without Derivatives. Prentice-Hall series in automatic computation, Prentice-Hall, Englewood Cliffs, NJ.
- Buhler, C.R., Calle, C.I., Nelson, E., 2003. Electrical breakdown in a Martian gas mixture, in: Mackwell, S., Stansbery, E. (Eds.), LPSC, LPI URSA, League City, TX.
- Chatain, A., Le Gall, A., Berthelier, J.J., Lorenz, R.D., Hassen-Khodja, R., Lebreton, J.P., Joly-Jehenne, T., Déprez, G., 2022. Detection and characterization of wind-blown charged sand grains on titan with the dragmet/efield experiment on dragonfly. *Icarus* , 115345.
- Chen, F.F., 1984. Introduction to Plasma Physics and Controlled Fusion. Plenum Press, New York.
- Cimarelli, C., Behnke, S., Genareau, K., Harper, J.M., Van Eaton, A.R., 2022. Volcanic electrification: recent advances and future perspectives. *Bulletin of Volcanology* 84, 1–10.
- Crozier, W.D., 1964. The electric field of a New Mexico dust devil. *J. Geophys. Res.* 69, 5427–5429. doi:10.1029/JZ069i024p05427.
- Delory, G., Farrell, W., 2011. Atmospheric electricity on Mars, in: EPSC-DPS Joint Meeting, p. 1229.
- Déprez, G., Montmessin, F., Witasse, O., Lapauw, L., Vivat, F., Abbaki, S., Granier, P., Moirin, D., Trautner, R., Hassen-Khodja, R., d’Almeida, É., Chardenal, L., Berthelier, J.J., Esposito, F., Debei, S., Rafkin, S., Barth,

- E., 2014. Micro-ARES, an electric-field sensor for ExoMars 2016: Electric fields modelling, sensitivity evaluations and end-to-end tests, in: EGU General Assembly Conference Abstracts, p. 16613.
- Dubrovín, D., Nijdam, S., van Veldhuizen, E.M., Ebert, U., Yair, Y., Price, C., 2010. Sprite discharges on Venus and Jupiter-like planets: A laboratory investigation. *J. Geophys. Res.* 115. doi:10.1029/2009ja014851.
- Dufek, J., Bergantz, G., 2007. Suspended load and bed-load transport of particle-laden gravity currents: the role of particle-bed interaction. *Theoretical and Computational Fluid Dynamics* 21, 119–145.
- Dufek, J., Manga, M., Patel, A., 2012. Granular disruption during explosive volcanic eruptions. *Nature Geoscience* 5, 561–564.
- Eden, H.F., Vonnegut, B., 1973. Electrical breakdown caused by dust motion in low pressure atmospheres: Considerations for Mars. *Nature* 280, 962.
- Farrell, W., McLain, J., Marshall, J., Wang, A., 2021. Will the mars helicopter induce local martian atmospheric breakdown? *The Planetary Science Journal* 2, 46.
- Farrell, W.M., Delory, G.T., Cummer, S.A., Marshall, J.R., 2003. A simple electrodynamic model of a dust devil. *Geophys. Res. Lett.* 30, 2050. doi:10.1029/2003GL017606.
- Farrell, W.M., Desch, M.D., 2001. Is there a Martian atmospheric electric circuit? *J. Geophys. Res.* 106, 7591–7596. doi:10.1029/2000JE001271.

- Farrell, W.M., Smith, P.H., Delory, G.T., Hillard, G.B., Marshall, J.R., Catling, D., Hecht, M., Tratt, D.M., Renno, N., Desch, M.D., Cummer, S.A., Houser, J.G., Johnson, B., 2004. Electric and magnetic signatures of dust devils from the 2000–2001 MATADOR desert tests. *J. Geophys. Res.* 109. doi:10.1029/2003JE002088. e03004.
- Forsythe, G.E., Malcolm, M.A., Moler, C.B., 1976. *Computer Methods for Mathematical Computations*. Automatic Computation, Prentice-Hall, Englewood Cliffs, NJ.
- Hackam, R., 1969. Total secondary ionization coefficients and breakdown potentials of hydrogen, methane, ethylene, carbon monoxide, nitrogen, oxygen and carbon dioxide between mild steel coaxial cylinders. *J. Phys. B: At. Mol. Phys.* 2, 216–233. doi:10.1088/0022-3700/2/2/309.
- Hagelaar, G.J.M., 2015. Coulomb collisions in the Boltzmann equation for electrons in low-temperature gas discharge plasmas. *Plasma Sources Sci. Technol.* 25, 015015. doi:10.1088/0963-0252/25/1/015015.
- Harrison, R.G., Barth, E., Esposito, F., Merrison, J., Montmessin, F., Aplin, K.L., Borlina, C., Berthelier, J.J., Déprez, G., Farrell, W.M., Houghton, I.M.P., Renno, N.O., Nicoll, K.A., Tripathi, S.N., Zimmerman, M., 2016. Applications of electrified dust and dust devil electro-dynamics to Martian atmospheric electricity. *Space Sci. Rev.* 203, 299–345. doi:10.1007/s11214-016-0241-8.
- Hayes, A.G., Lorenz, R.D., Lunine, J.I., 2018. A post-cassini view of titan’s methane-based hydrologic cycle. *Nature Geoscience* 11, 306–313.

- Hess, B.L., Piazzolo, S., Harvey, J., 2021. Lightning strikes as a major facilitator of prebiotic phosphorus reduction on early earth. *Nature communications* 12, 1–8.
- Horányi, M., Lawrence, G., 2001. Charged dust currents on the surface of Mars. *Phys. Scr.* 89, 130–132. doi:10.1238/Physica.Topical.089a00130.
- Hörst, S.M., 2017. Titan’s atmosphere and climate. *Journal of Geophysical Research: Planets* 122, 432–482.
- Jakosky, B.M., Grebowsky, J.M., Luhmann, J.G., Connerney, J., Eparvier, F., Ergun, R., Halekas, J., Larson, D., Mahaffy, P., McFadden, J., Mitchell, D.F., Schneider, N., Zurek, R., Bougher, S., Brain, D., Ma, Y.J., Mazelle, C., Andersson, L., Andrews, D., Baird, D., Baker, D., Bell, J.M., Benna, M., Chaffin, M., Chamberlin, P., Chaufray, Y.Y., Clarke, J., Collinson, G., Combi, M., Crary, F., Cravens, T., Crismani, M., Curry, S., Curtis, D., Deighan, J., Delory, G., Dewey, R., DiBraccio, G., Dong, C., Dong, Y., Dunn, P., Elrod, M., England, S., Eriksson, A., Espley, J., Evans, S., Fang, X., Fillingim, M., Fortier, K., Fowler, C.M., Fox, J., Gröller, H., Guzewich, S., Hara, T., Harada, Y., Holsclaw, G., Jain, S.K., Jolitz, R., Leblanc, F., Lee, C.O., Lee, Y., Lefevre, F., Lillis, R., Livi, R., Lo, D., Mayyasi, M., McClintock, W., McEnulty, T., Modolo, R., Montmessin, F., Morooka, M., Nagy, A., Olsen, K., Peterson, W., Rahmati, A., Ruhunusiri, S., Russell, C.T., Sakai, S., Sauvaud, J.A., Seki, K., Steckiewicz, M., Stevens, M., Stewart, A.I.F., Stiepen, A., Stone, S., Tennishev, V., Thiemann, E., Tolson, R., Toubanc, D., Vogt, M., Weber, T., Withers, P., Woods, T., Yelle, R.,

- 2015a. MAVEN observations of the response of Mars to an interplanetary coronal mass ejection. *Science* 350, 0210. doi:10.1126/science.aad0210.
- Jakosky, B.M., Lin, R.P., Grebowsky, J.M., Luhmann, J.G., Mitchell, D., Beutelschies, G., Priser, T., Acuna, M., Andersson, L., Baird, D., et al., 2015b. The mars atmosphere and volatile evolution (maven) mission. *Space Science Reviews* 195, 3–48.
- James, M., Wilson, L., Lane, S., Gilbert, J., Mather, T., Harrison, R., Martin, R., 2008. Electrical charging of volcanic plumes. *Space Science Reviews* 137, 399–418.
- Justh, H., Hoffman, J., 2020. Titan global reference atmospheric model (titan-gram): User guide .
- Justh, H.L., Dwyer Cianciolo, A., 2021. Venus Global Reference Atmospheric Model (Venus-GRAM) updates, in: 43rd COSPAR Scientific Assembly, p. 429. URL: <https://ui.adsabs.harvard.edu/abs/2021cosp...43E.429J>. 28 January - 4 February.
- Justh, H.L., Justus, C.G., Badger, A.M., 2010. Updating Mars-GRAM to increase the accuracy of sensitivity studies at large optical depths, in: COSPAR Scientific Assembly, p. 4.
- Kamra, A., 1972. Physical sciences: Visual observation of electric sparks on gypsum dunes. *Nature* 240, 143–144.
- Krauss, C.E., Horányi, M., Robertson, S., 2003. Experimental evidence for electrostatic discharging of dust near the surface of Mars. *New J. Phys.* 5, 70. doi:10.1088/1367-2630/5/1/370.

- Leblanc, F., Aplin, K., Yair, Y., Harrison, G., Lebreton, J.P., Blanc, M. (Eds.), 2008. Planetary Atmospheric Electricity. Space Sciences Series of ISSI, Springer-Verlag GmbH, New York, NY.
- Leslie, F., 2008. Earth Global Reference Atmospheric Model 2007 (Earth-GRAM07), in: COSPAR Scientific Assembly, p. 1748.
- Lieberman, M.A., Lichtenberg, A.J., 2005. Principles of Plasma Discharges and Materials Processing. Second ed., John Wiley & Sons, Inc., New York, NY.
- Lipschutz, S., Spiegel, M., Liu, J., 2018. Schaum's Outline of Mathematical Handbook of Formulas and Tables. 5 ed., McGraw-Hill Ed. URL: https://www.ebook.de/de/product/29116254/seymour_lipschutz_murray_spiegel_john_liu_schaum_s_outline_of_mathematical_handbook_of_formulas_and_tables_fifth_edition.html.
- Lorenz, R.D., Zimbelman, J.R., 2014. Venus dunes, in: Dune Worlds. Springer, pp. 169–176.
- Lowke, J.J., D'Alessandro, F., 2003. Onset corona fields and electrical breakdown criteria. *J. Phys. D: Appl. Phys.* 36, 2673–2682. doi:10.1088/0022-3727/36/21/013.
- Manning, H.L.K., ten Kate, I.L., Battel, S.J., Mahaffy, P.R., 2010. Electric discharge in the Martian atmosphere, Paschen curves and implications for future missions. *Adv. Space Res.* 46, 1334–1340. doi:10.1016/j.asr.2010.07.006.

- Meek, J.M., Craggs, J.D., 1953. *Electrical Breakdown of Gases*. International series of monographs on physics. first ed., Clarendon Press, Oxford, UK.
- Melnik, O., Parrot, M., 1998. Electrostatic discharge in Martian dust storms. *J. Geophys. Res.* 103, 29107–29118. doi:10.1029/98JA01954.
- Méndez Harper, J., Dufek, J., McDonald, G.D., 2021. Detection of spark discharges in an agitated mars dust simulant isolated from foreign surfaces. *Icarus* 357, 114268.
- Méndez Harper, J., Harvey, D., Huang, T., McGrath III, J., Meer, D., Burton, J.C., 2022. The lifetime of charged dust in the atmosphere. *PNAS Nexus* 1, pgac220.
- Méndez Harper, J., Helling, C., Dufek, J., 2018. Triboelectrification of KCl and ZnS particles in approximated exoplanet environments. *Astrophys. J.* 867, 123. doi:10.3847/1538-4357/aadf36.
- Méndez Harper, J.S., McDonald, G.D., Dufek, J., Malaska, M.J., Burr, D.M., Hayes, A.G., McAdams, J., Wray, J.J., 2017. Electrification of sand on Titan and its influence on sediment transport. *Nat. Geosci.* 10, 260–265. doi:10.1038/ngeo2921.
- Merrison, J., Jensen, J., Kinch, K., Mugford, R., Nørnberg, P., 2004. The electrical properties of Mars analogue dust. *Planet. Space Sci.* 52, 279–290. doi:10.1016/j.pss.2003.11.003.
- Moore, C.B., 1983. Improved configurations of lightning rods and air terminals. *J. Franklin Inst.* 315, 61–85. doi:10.1016/0016-0032(83)90107-2.

- Moore, C.B., Aulich, G.D., Rison, W., 2000a. Measurements of lightning rod responses to nearby strikes. *Geophys. Res. Lett.* 27, 1487–1490. doi:10.1029/1999GL011053.
- Moore, C.B., Aulich, G.D., Rison, W., 2003. The case for using blunt-tipped lightning rods as strike receptors. *J. Appl. Meteorol. Climatol.* 42, 984–993. doi:10.1175/1520-0450(2003)042<0984:TCFUBL>2.0.CO;2.
- Moore, C.B., Rison, W., Mathis, J., Aulich, G., 2000b. Lightning rod improvement studies. *J. Appl. Meteorol. Climatol.* 39, 593–609. doi:10.1175/1520-0450-39.5.593.
- Naidu, M.S., Kamaraju, V., 2013. *High Voltage Engineering*. Fifth ed., McGraw Hill, New York, NY.
- Paschen, F., 1889. Über die zum Funkenübergang in Luft, Wasserstoff und Kohlensäure bei verschiedenen Drucken erforderliche Potentialdifferenz. *Ann. Phys.* 273, 69–96. doi:10.1002/andp.18892730505.
- Pasko, V.P., 2006. Theoretical Modeling of Sprites and Jets, in: Füllekrug, M., Mareev, E.A., Rycroft, M.J. (Eds.), *Sprites, Elves and Intense Lightning Discharges*. Kluwer Academic Publishers, Heidelberg, Germany. volume 225, pp. 253–311. doi:10.1007/1-4020-4629-4_12.
- Radebaugh, J., Lorenz, R., Lunine, J., Wall, S., Boubin, G., Reffet, E., Kirk, R.L., Lopes, R., Stofan, E., Soderblom, L., et al., 2008. Dunes on titan observed by cassini radar. *Icarus* 194, 690–703.
- Raizer, Y.P., 1991. *Gas Discharge Physics*. Springer-Verlag, New York, NY.

- Riousset, J.A., Nag, A., Palotai, Cs., 2020. Scaling of conventional breakdown threshold: Impact for predictions of lightning and TLEs on Earth, Venus, and Mars. *Icarus* 338, 113506. doi:10.1016/j.icarus.2019.113506.
- Sánchez-Lavega, A., Lebonnois, S., Imamura, T., Read, P., Luz, D., 2017. The atmospheric dynamics of venus. *Space Science Reviews* 212, 1541–1616.
- Shao, W.D., Zhang, X., Bierson, C.J., Encrenaz, T., 2020. Revisiting the sulfur-water chemical system in the middle atmosphere of venus. *Journal of Geophysical Research: Planets* 125, e2019JE006195.
- Stumbo, M.T., 2013. Paschen Breakdown in a CO₂ Atmosphere. Cal. Poly., San Luis Obispo, CA. URL: <http://digitalcommons.calpoly.edu/aerosp/114>. B.Sc. Thesis.
- Tennakone, K., 2016. Contact electrification of regolith particles and chloride electrolysis: synthesis of perchlorates on mars. *Astrobiology* 16, 811–816.
- Thomas, P., Gierasch, P.J., 1985. Dust devils on mars. *Science* 230, 175–177.
- Townsend, J.S., 1900. The conductivity produced in gases by the motion of negatively-charged ions. *Nature* 62, 340–341. doi:10.1038/062340b0.
- Townsend, J.S., 1901. XVII. The conductivity produced in gases by the motion of negatively charged ions. *Philos. Mag.* 1, 198–227. doi:10.1080/14786440109462605.
- Uman, M.A., 2001. *The Lightning Discharge*. Unabridged ed., Dover, Mineola, NY.

- Wurm, G., Schmidt, L., Steinpilz, T., Boden, L., Teiser, J., 2019. A challenge for martian lightning: Limits of collisional charging at low pressure. *Icarus* 331, 103–109. doi:10.1016/j.icarus.2019.05.004.
- Yair, Y., 2012. New results on planetary lightning. *Adv. Space Res.* 50, 293–310. doi:10.1016/j.asr.2012.04.013.
- Zangwill, A., 2019. *Modern Electrodynamics*. Cambridge Univ. Press.
- Zasova, L., Ignatiev, N., Khatuntsev, I., Linkin, V., 2007. Structure of the venus atmosphere. *Planetary and Space Science* 55, 1712–1728.